Fundamental Electromagnetic Emissions by a Weak Electron Beam in Solar Wind Plasmas with Density Fluctuations

C. Krafft and P. Savoini
Laboratoire de Physique des Plasmas (LPP), CNRS, Sorbonne Université, Observatoire de Paris, Université Paris-Saclay, École polytechnique, Institut Polytechnique de Paris, F-91128 Palaiseau, France; catherine.krafft@universite-paris-saclay.fr

Abstract

The generation of Langmuir wave turbulence by a weak electron beam in a randomly inhomogeneous plasma and its subsequent electromagnetic radiation are studied owing to two-dimensional particle-in-cell simulations in conditions relevant to type III solar radio bursts. The essential impact of random density fluctuations of average levels of a few percents of the background plasma on the characteristics of the electromagnetic radiation at the fundamental plasma frequency ω_p is shown. Not only wave nonlinear interactions but also processes of Langmuir waves' transformations on the density fluctuations contribute to the generation of such emissions. During the beam relaxation, the amount of electromagnetic energy radiated at ω_p in a plasma with density fluctuations strongly exceeds that observed when the plasma is homogeneous. The fraction of Langmuir wave energy involved in the generation of electromagnetic emissions at ω_p saturates around 10^{-4}, i.e., one order of magnitude above that reached when the plasma is uniform. Moreover, whereas harmonic emission at $2\omega_p$ dominates over fundamental emission during the time evolution in a homogeneous plasma, fundamental emission is strongly dominant when the plasma contains density fluctuations, at least during several thousands of plasma periods before being overcome by harmonic emission when the total electromagnetic energy begins to saturate.

Unified Astronomy Thesaurus concepts: Solar electromagnetic emission (1490); Solar wind (1534); Radio bursts (1339)

1. Introduction

Type III solar radio bursts have been observed for decades in interplanetary space (Reid & Ratcliffe 2014). They result from a series of successive processes arising in solar coronal and wind plasmas where Langmuir wave turbulence is radiated by electron beams generated during flares, leading ultimately to the emission of electromagnetic waves at the fundamental plasma frequency ω_p and its second harmonic.

Electromagnetic wave radiation at ω_p was first believed to arise from Langmuir waves scattering off thermal ions (Ginzburg & Zheleznyakov 1958). Later, various approaches were suggested to elucidate the mechanisms responsible for the generation of such electromagnetic waves. In the frame of weak turbulence theory, it was proposed (Melrose 1980) that they arise from nonlinear wave decay or fusion processes $\mathcal{L} \pm \mathcal{S} \rightarrow \mathcal{F}$ involving Langmuir waves $\mathcal{L}$, ion acoustic waves $\mathcal{S}$, and electromagnetic waves $\mathcal{F}$ radiated at ω_p. The theory of strong turbulence was also invoked (Papadopoulos et al. 1974) by considering, for example, electromagnetic emissions by cavitons containing trapped Langmuir waves. However, linear processes were shown to partly account for such electromagnetic radiations, i.e., transformations of Langmuir waves on plasma inhomogeneities (Field 1956). Such conversion processes were studied numerically and analytically by considering monochromatic waves incident on density gradients (e.g., Yin et al. 1998; Cairns & Willes 2005) or wave scattering on external density fluctuations (Volokitin & Krafft 2018, 2020).

On the numerical point of view, electromagnetic emissions at ω_p were studied by solving the weak turbulence equations (Li et al. 2005; Ziebell et al. 2015; Lee et al. 2019), the Zhakarov equations coupled with a modified theory of retarded potentials in plasmas with density fluctuations (Volokitin & Krafft 2018; Krafft & Volokitin 2020), or within the framework of two-dimensional (2D) particle-in-cell (PIC) simulations (Kasaba et al. 2001; Rhee et al. 2009; Thurgood & Tsiklauri 2015; Lee et al. 2019).

The Letter presents 2D PIC simulations showing for the first time the radiation in randomly inhomogeneous plasmas of electromagnetic waves emitted at ω_p by Langmuir wave turbulence generated by a weak electron beam. These simulations use a panel of physical and numerical parameters that were not reached in previous works and take into account the presence of applied and self-consistently varying random plasma density fluctuations (Celnikier et al. 1983; Krupar et al. 2018) in an exceptionally large and well-resolved simulation box.

This study shows the essential impact of plasma density fluctuations on the intensity, the rate of growth, and the spectral distributions of the fundamental electromagnetic emissions. Moreover, it demonstrates that not only three-waves' nonlinear interactions contribute to their generation in solar wind plasmas, but also processes involving Langmuir waves' transformations on the background plasma inhomogeneities.

2. Simulation Parameters

The results presented below are provided by three simulations using two different spatial boxes (designated as "large box" or "smaller box") and two values of average levels $\Delta N = \langle (\delta n/n_0)^2 \rangle^{1/2}$ of density fluctuations (n_0 is the density of the background ions), i.e., $\Delta N = 0$ for a homogeneous plasma and $\Delta N = 0.05$ for a plasma involving random fluctuations δn
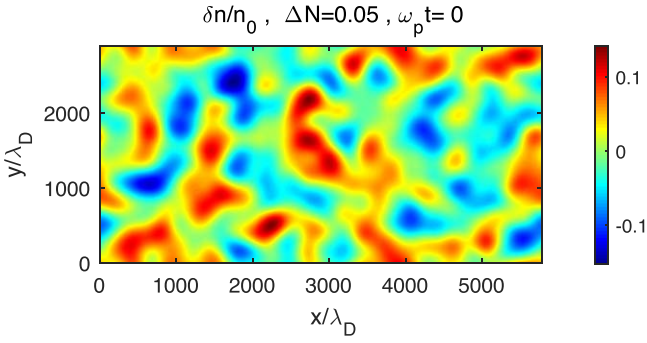
Figure 1. Initial distribution of the background plasma density fluctuations $\delta n/n_0$ in the plane (x, y), corresponding to the average level $\Delta N = \langle (\delta n/n_0)^2 \rangle^{1/2} \simeq 0.05$. The size of the box is $L_x \times L_y = 5792 \times 2896 \lambda_D^2$.

of wavelengths much larger than the Langmuir waves' ones. These density distributions result from 2D Gaussian spectra $\delta n_k(k_x, k_y)$ with random phases, are applied initially, and evolve self-consistently.

The size of the "large" ("smaller") simulation box is given by $L_x \times L_y = 5792 \times 2896 \lambda_D^2$, with $N_x = 4096$ and $N_y = 2048$ grid points ($L_x \times L_y = 1448 \times 1448 \lambda_D^2$, with $N_x = N_y = 1024$) and spatial cells $\Delta x = \Delta y = \sqrt{2} \lambda_D$; λ_D is the electron Debye length. Both boxes contain $N_c = 1800$ particles per species and per cell. Three species are considered, i.e., the beam electrons (of density n_b), as well as the background electrons and ions (of density $n_e = n_0 - n_b$ and n_0, respectively); the quasineutrality is ensured by assigning a statistical weight to each macroparticle. The large number of particles per cell reduces the numerical noise below 10^{-2}, i.e., significantly below ΔN.

For the "large" ("smaller") boxes, the normalized wave-number resolutions are $\delta k_x \lambda_D = 0.001$ and $\delta k_y \lambda_D = 0.002$ ($\delta k_{x,y} \lambda_D = 0.004$), to be compared with the theoretical wave vectors' moduli $k_{th} \lambda_D = \sqrt{3} (k_L \lambda_D) v_T/c \simeq 0.004$ of the electromagnetic waves emitted at ω_p through nonlinear wave processes; k_L is the characteristic wave vector of the Langmuir waves generated by the beam propagating along the x-axis with the initial drift velocity v_b. Considering parameters typical of type III radio-burst regions in weakly magnetized solar wind and coronal plasmas, we choose $v_b = 9 v_T = 0.25c$, where $v_T = 0.028c$ and $v_{T_b} = v_T$ are the background plasma and beam thermal velocities. The ratio $T_i/T_e = 0.1$ of the ion to the electron plasma temperatures prevents ion acoustic wave damping. Long computations (up to $8000 \omega_p^{-1}$) are necessary to follow the complete dynamics of the weak electron beam of density $n_b = 5 \times 10^{-4} n_0$.

The simulations are carried out using the 2D–3V version of the open-source relativistic full PIC code SMILEI (Derouillat et al. 2018). A realistic mass ratio $m_p/m_e = 1836$ is used, where m_e and m_p are the electron and proton masses. The particle velocity distributions of the beam and the plasma are initially Maxwellians; the background electron population is shifted by a small velocity to keep a net zero current. During the simulations, over roughly 10^6 time steps, the relative variation of the total energy remains below 2×10^{-4}. The turbulence parameter does not exceed 10^{-2} so that the role of ponderomotive effects is negligible.

Figure 1 shows the initial distribution of the background plasma density fluctuations $\delta n/n_0$ in the plane (x, y) used for the "large" simulation box mentioned above, for $\Delta N \simeq 0.05$.

## 3. Electromagnetic Emissions

Numerical calculations are presented hereafter for both homogeneous and randomly inhomogeneous plasmas, with the two-fold aim of presenting spectral emissions of unprecedented accuracy and resolution and highlighting for the first time the impact of the background density fluctuations on the processes responsible for the electromagnetic wave radiation at the fundamental frequency ω_p. Below time, space, and velocity are normalized by ω_p, λ_D, and v_T, respectively; the electric and magnetic fields E and B are presented in dimensionless forms, $eE/(m_e c \omega_p)$ and $eB/(m_e \omega_p)$, where e is the electron charge.

Figure 2 shows, at different times, the distributions of the magnetic energy density $|B_{zk}(k_x, k_y)|^2$ of waves emitted at $\omega_k \simeq \omega_p$, for $\Delta N = 0.05$ and the "large" simulation box; B_{zk} is the Fourier transform of the magnetic field component $B_z(x, y)$; k_x and k_y are the parallel and perpendicular components of the wave vector k, respectively. In order to compare each spectrum of Figure 2 with the others, the same color bar is fixed for all plots. Electromagnetic emissions already appear at early times before Langmuir wave saturation (occurring near $\omega_p t \simeq 1000$), revealing a circularly distributed wave excitation pattern roughly scattered within the spectral region $0.004 \lesssim k\lambda_D \lesssim 0.01$. Note that, according to theory developed in unmagnetized and uniform plasmas, the wave vectors of the electromagnetic waves produced at $\omega_k \simeq \omega_p$ via wave nonlinear processes through the channels $\mathcal{L} \pm \mathcal{S} \to \mathcal{F}$ satisfy here $k_{th} \lambda_D \simeq 0.004$ (see the green circles), with the estimate $k_L \lambda_D \sim 0.1$. When time increases, the electromagnetic emissions are strongly scattered around a quasi-isotropic circular shape, covering the region $0.002 \lesssim k\lambda_D \lesssim 0.04$, which is consistent with the development of Langmuir wave decay $\mathcal{L} \to \mathcal{F} + \mathcal{S}$ or nonlinear-induced scattering $\mathcal{L} + \mathcal{S} \to \mathcal{F}$ during beam relaxation, as well as with wave transformations on density fluctuations responsible for wave energy diffusion in k-space. Eventually, the emissions are isotropically distributed in the spectral domain $0.001 \lesssim k\lambda_D \lesssim 0.01$, with no visible radiation at $k\lambda_D \lesssim 0.001$ (see the central pixel).

Figures 3(a)–(b) show the spectra $|B_{zk}(k_x, k_y)|^2$ obtained at similar times and parameters, using the "smaller" simulation box, for $\Delta N = 0$ (Figure 3(a)) and $\Delta N = 0.05$ (Figure 3(b)). Comparing Figures 3(a) and 2–3(b) reveals clearly the strong impact of density fluctuations on the intensity and the spectral distribution of the electromagnetic emissions at ω_p. In particular, at early times, $|B_{zk}|^2$ is several orders of magnitude larger for $\Delta N = 0.05$ than for $\Delta N = 0$. In the latter case, however, $|B_{zk}|^2$ grows continuously with time, presenting a quasicircular shape of average radius $k\lambda_D \simeq 0.005$, with maxima appearing near $(k_x\lambda_D, k_y\lambda_D) \simeq (0, \pm 0.005)$, in agreement with the theoretical angular distribution of the nonlinear coupling coefficient of the wave-interaction processes $\mathcal{L} \pm \mathcal{S} \to \mathcal{F}$, which is proportional to $\sin^2 \theta$, where θ is the angle between the electromagnetic and the Langmuir wave vectors (e.g., Ziebell et al. 2015). Then Figure 3(a) exhibits for the uniform plasma the expected dipolar radiation structure at all times, only not at $\omega_p t = 145$ where the emission is very weak. This property is not observed in the presence of density fluctuations, as the scattering phenomena contribute to isotropize the emission patterns.
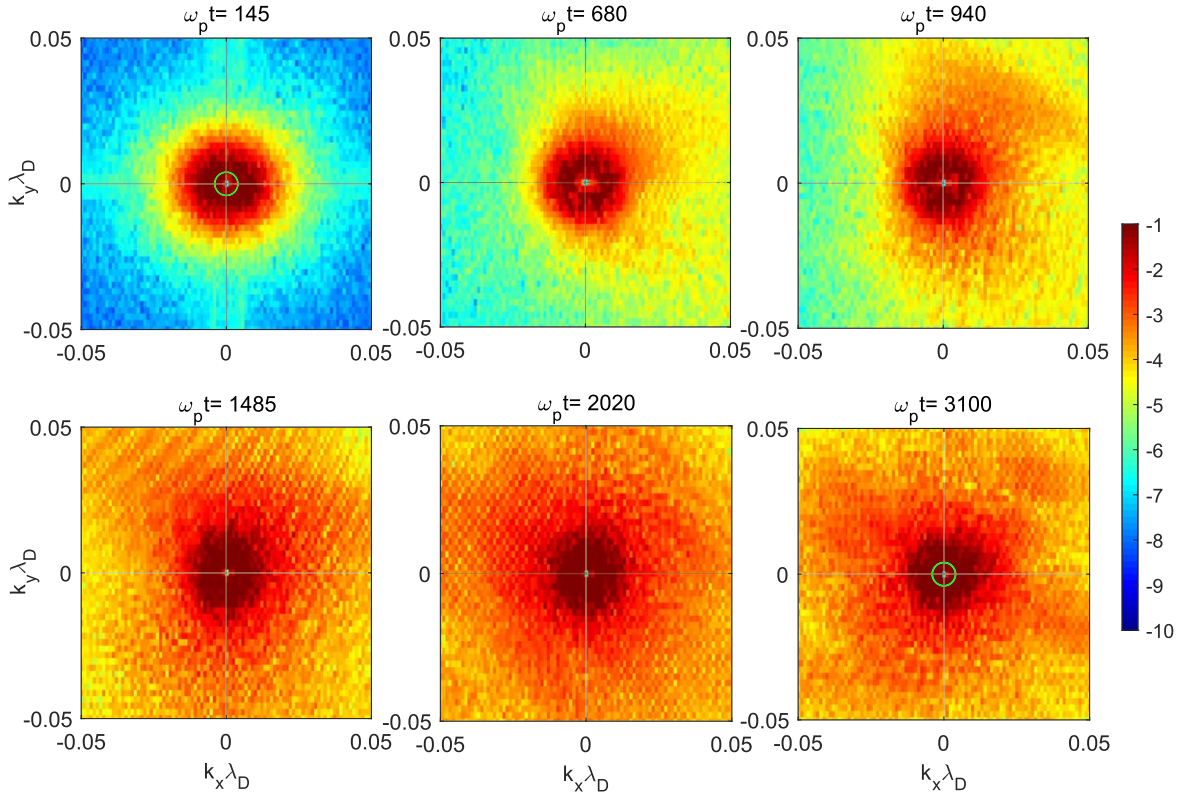
Figure 2. Distributions of the wave spectral magnetic energy density $\log_{10}(|B_{zk}(k_x, k_y)|^2)$ emitted around the frequency $\omega_k \simeq \omega_p$, for $\Delta N = 0.05$ and the "large" simulation box of size $L_x \times L_y = 5792 \times 2896\lambda_D^2$. The initial plasma density distribution is given in Figure 1. The spectra are shown at times $\omega_p t = 145, 680, 940, 1485, 2020,$ and 3100. A green circle of radius $k\lambda_D \simeq k_{th}\lambda_D$ is superposed on the spectra at the first and last times. The same color bar holds for all plots. All variables are normalized.
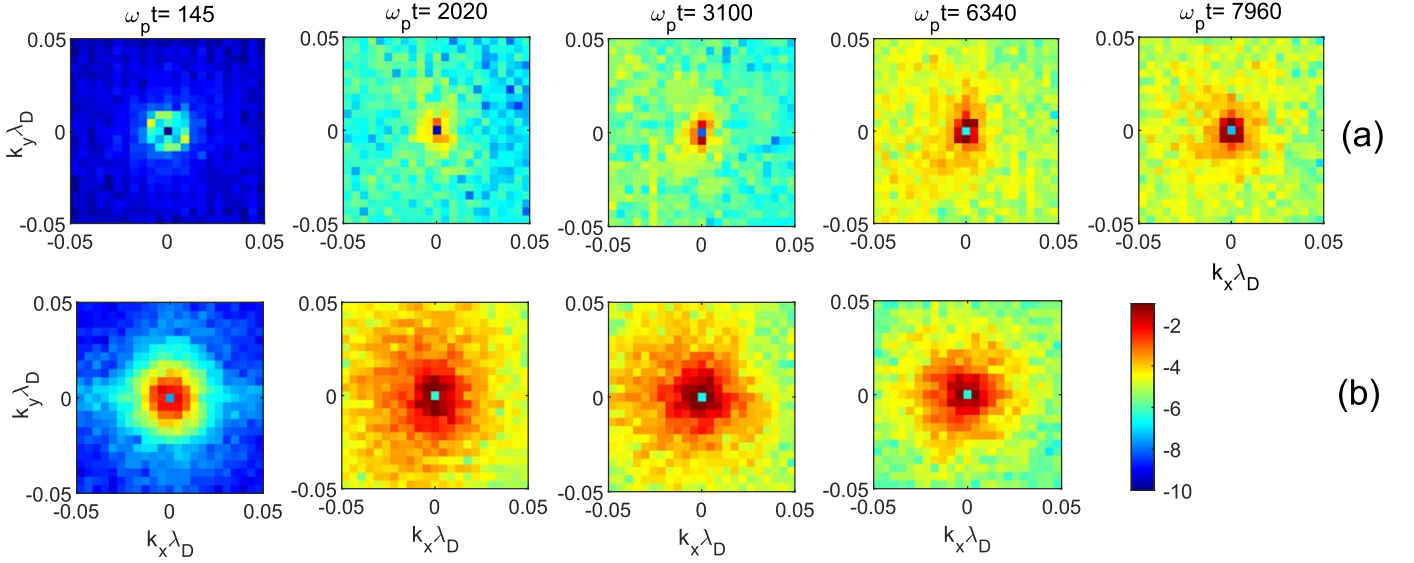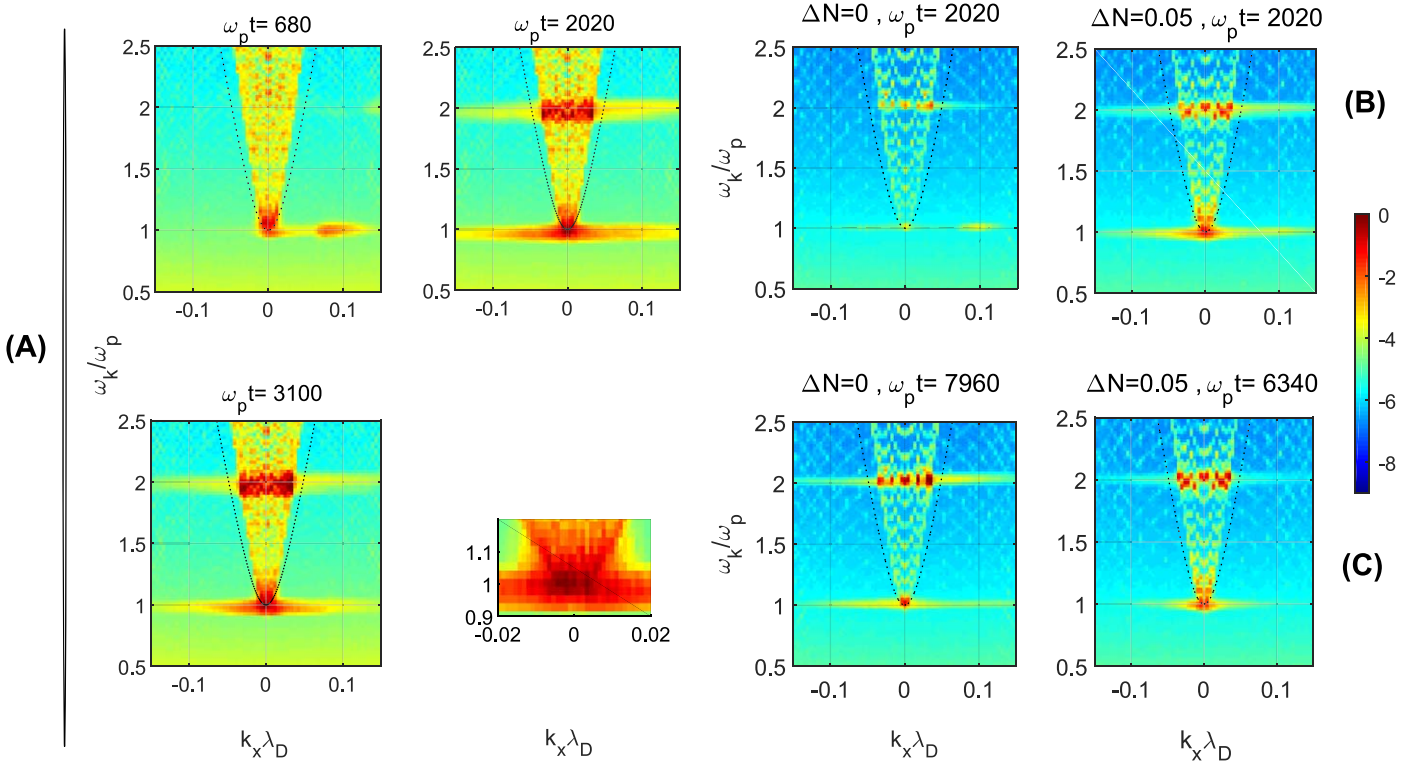

Figure 3. Distributions of the wave spectral magnetic energy densities $\log_{10}(|B_{zk}(k_x, k_y)|^2)$ emitted at the frequency $\omega_k \simeq \omega_p$, for (a) $\Delta N = 0$ (upper row) and (b) $\Delta N = 0.05$ (bottom row). The initial density distribution is given in Figure 1 of Krafft & Savoini (2021). The "smaller" box with size $L_x \times L_y = 1448 \times 1448\lambda_D^2$ is used. The spectra are given at times $\omega_p t = 145, 2020, 3100, 6430,$ and 7960. The same color bar holds for all plots. All variables are normalized.

Comparing Figures 2 and 3(b), which only differ from one another by the size and the resolution of the simulation box used, one observes similar qualitative features, even if Figure 2 provides much more detail. Moreover, at $\omega_p t \gtrsim 3000$ (not shown in Figure 2 due to computing resources), emissions tend to isotropize and when time increases, they tend to decrease in intensity due to the continuous damping of the total Langmuir

wave energy after its saturation near $\omega_p t \simeq 1000$ (see also Figure 5(a)). Asymptotically, one observes a quasicircular structure of maximum intensity near $k\lambda_D \simeq 0.005 \simeq k_{th}\lambda_D$ (dark red regions surrounding the blue pixel at $\omega_p t \simeq 7960$ (Figure 3(a)) and $\omega_p t \simeq 6340$ (Figure 3(b))).

Figure 4 presents the corresponding wave-dispersion plots for $\Delta N = 0$ and $\Delta N = 0.05$. The spectral energy density

Figure 4. Dispersion plots of the wave spectral magnetic energy densities $\log_{10}(|B_{zk}(\omega_k, k_x)|^2)$ as a function of the normalized frequency ω_k/ω_p and parallel wave vector $k_x\lambda_D$, for a homogeneous plasma with $\Delta N = 0$ and a plasma with density fluctuations ($\Delta N = 0.05$). The simulations used are the same as in Figures 2–3. Panel A: dispersion plots for $\Delta N = 0.05$, at $\omega_p t = 680$, 2020, and 3100, computed with the "large" simulation box; a zoom of the frequency wave-number domain $0.9 < \omega_k/\omega_p < 1.2$ and $|k_x\lambda_D| < 0.02$ is shown for $\omega_p t = 3100$ in the bottom right corner. Panel B : dispersion plots obtained using the "smaller" box, at $\omega_p t = 2020$, for $\Delta N = 0$ (left) and $\Delta N = 0.05$ (right). Panel C: dispersion plots at asymptotic times for $\Delta N = 0$ (left, $\omega_p t = 7960$) and $\Delta N = 0.05$ (right, $\omega_p t = 6340$); the "smaller" simulation box is used. The same color bar holds for all plots of panels (A), (B), and (C). All variables are normalized.

$|B_{zk}(\omega_k, k_x)|^2$ is shown versus ω_k/ω_p and $k_x\lambda_D$. For better visibility of emissions at $\omega_k \simeq \omega_p$ and $\omega_k \simeq 2\omega_p$, we selected the ranges $0.5 < \omega_k/\omega_p < 2.5$ and $|k_x\lambda_D| < 0.15$. The black dotted lines represent the theoretical dispersion relations $\omega_k^2 = \omega_{p0}^2 + k^2c^2$ of parallel propagating electromagnetic waves ($k = k_x$) in an unmagnetized uniform plasma of density n_0, with $\omega_{p0}^2 = n_0e^2/\varepsilon_0 m_e$. For $\Delta N = 0.05$ and simulations using the "large" box, panel (A) shows the presence, at $\omega_p t = 680$, of strong and scattered electromagnetic emissions at $|k_x\lambda_D| \lesssim 0.02$ and $0.9 \lesssim \omega_k/\omega_p \lesssim 1.2$. The emissions of largest intensity satisfy $1 \lesssim \omega_k/\omega_p \lesssim 1.1$ and lie on dispersion curves of electromagnetic waves propagating oblique to the beam direction. Moreover, some excitation near $k_x\lambda_D \simeq 0.07 - 0.09$ and $\omega_k/\omega_p \simeq 1$ is visible, which is the so-called beam mode appearing due to beam instability enhancement (Pritchett & Dawson 1983), also observable for $\Delta N = 0$. At $\omega_p t = 2020$ and 3100, emissions within the domains $0.97 \lesssim \omega_k/\omega_p \lesssim 1.07$ and $|k_x\lambda_D| \lesssim 0.005$ are enhanced, with a maximum intensity near $\omega_k/\omega_p \simeq 1$ (see the zoom for $\omega_p t = 3100$), and extend with weaker amplitudes up to $|k_x\lambda_D| \simeq 0.04$ and within $0.9 \lesssim \omega_k/\omega_p \lesssim 1$, whereas harmonic electromagnetic waves appear at frequencies $1.9 \lesssim \omega_k/\omega_p \lesssim 2.1$.

Let us compare the dispersion plot at $\omega_p t = 2020$ (Figure 4, panel (A)) with those obtained at the same time using the "smaller" box, for $\Delta N = 0$ and $\Delta N = 0.05$ (panel (B)). For $\Delta N = 0$, the most intense emissions occur at $\omega_k \simeq 2\omega_p$, the radiation at $\omega_k \simeq \omega_p$ being at least two orders of magnitude weaker. For $\Delta N = 0.05$, the dispersion shows the same features than obtained using the "large" box (panel (A)) and highlights the strong intensification of fundamental emissions due to the

presence of density fluctuations. Finally, panel (C) presents the dispersion plots at asymptotic times, showing rather comparable intensities between emissions for $\Delta N = 0$ and $\Delta N = 0.05$, at $\omega_k = \omega_p$ and at $\omega_k = 2\omega_p$, with, however, more scattered frequencies and wave numbers in the inhomogeneous plasma case. Note for $\Delta N = 0$ the presence of weak electromagnetic harmonic emissions extending from $|k_x\lambda_D| \simeq 0.03$ up to larger wave numbers, which could be nonlinear eigenmodes as studied in Yoon et al. (2005).

Figure 5 presents the time variations of various energies W (integrated on the plasma volume) with the subscripts $\mathcal{L}$, $\mathcal{M}$, $\mathcal{F}$, $\mathcal{H}$, and h, indicating, respectively "total Langmuir," "total electromagnetic (including all frequencies)," "fundamental electromagnetic (at $\omega_k \simeq \omega_p$)," "harmonic electromagnetic (at $\omega_k \simeq 2\omega_p$)," and "homogeneous (plasma)"; without the subscript h, W refers to the inhomogeneous plasma case with $\Delta N = 0.05$. Note that here all energies are normalized by the initial beam kinetic energy.

Figure 5(a) shows the variations with time of the total Langmuir and electromagnetic wave energies, designated by $W_{\mathcal{L}h}$ and $W_{\mathcal{M}h}$ for the homogeneous plasma with $\Delta N = 0$ and by $W_{\mathcal{L}}$ and $W_{\mathcal{M}}$ for the plasma with $\Delta N = 0.05$. After quasisimilar growths, $W_{\mathcal{L}h}$ stabilizes around a constant level whereas $W_{\mathcal{L}}$ begins to decrease just after saturation, due namely to the beam dynamics (Krafft et al. 2013, 2015). Meanwhile, $W_{\mathcal{M}}$ reaches around $3 \ 10^{-5}$ asymptotically ($\omega_p t \simeq 6340$), after a stage of slow and continuous increase in spite of the corresponding damping of $W_{\mathcal{L}}$, remaining larger than $W_{\mathcal{M}h}$ until $\omega_p t \simeq 5000$; then $W_{\mathcal{M}h}$ becomes dominant and stabilizes asymptotically around 10^{-4}.
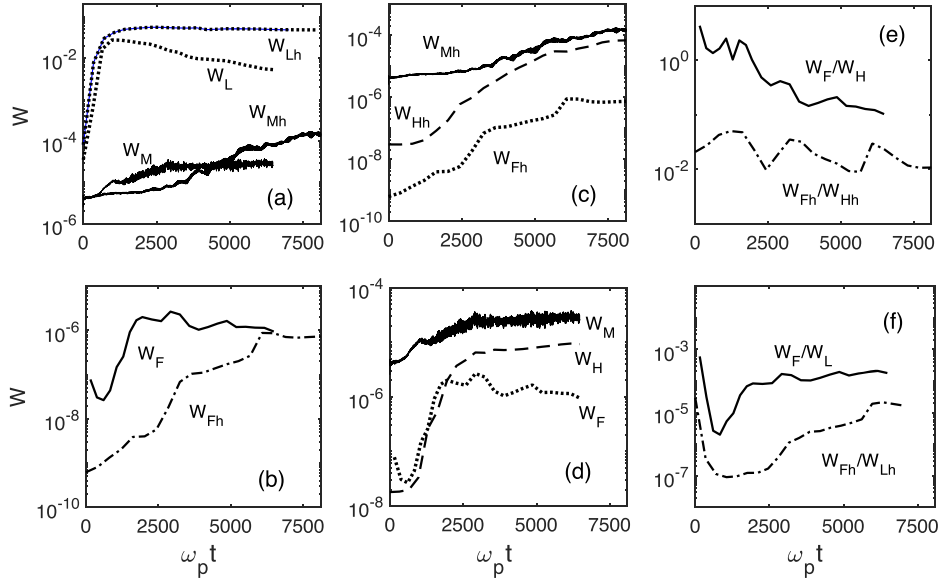
Figure 5. Time variations of various energies W in logarithmic scales. (a) : $W_{\mathcal{L}h}$ and $W_{\mathcal{M}h}$ as well as $W_{\mathcal{L}}$ and $W_{\mathcal{M}}$; the presence (absence) of the subscript "h" refers to the case of the homogeneous plasma (inhomogeneous plasma with $\Delta N = 0.05$); the subscripts "$\mathcal{L}$" and "$\mathcal{M}$" refer to the total Langmuir and the total electromagnetic energies, respectively. (b) : $W_{\mathcal{F}h}$ and $W_{\mathcal{F}}$; the subscript "$\mathcal{F}$" refers to the electromagnetic energy at frequency $\omega_k = \omega_p$. (c) : $W_{\mathcal{M}h}$, $W_{\mathcal{H}h}$, and $W_{\mathcal{F}h}$ (solid, dashed, and dotted curves), for $\Delta N = 0$; the subscript "$\mathcal{H}$" refers to the electromagnetic energy at frequency $\omega_k = 2\omega_p$. (d) : $W_{\mathcal{M}}$, $W_{\mathcal{H}}$, and $W_{\mathcal{F}}$ (solid, dashed, and dotted curves), for $\Delta N = 0.05$. (e) : $W_{\mathcal{F}h}/W_{\mathcal{H}h}$ and $W_{\mathcal{F}}/W_{\mathcal{H}}$. (f) : $W_{\mathcal{F}h}/W_{\mathcal{L}h}$ and $W_{\mathcal{F}}/W_{\mathcal{L}}$. All energies are normalized by the initial beam kinetic energy.

Figure 5(b) shows the time variation of the energy $W_{\mathcal{F}}$ ($W_{\mathcal{F}h}$) radiated at ω_p for $\Delta N = 0.05$ ($\Delta N = 0$). Whereas $W_{\mathcal{F}h}$ grows continuously over several orders of magnitude up to 10^{-6} asymptotically, $W_{\mathcal{F}}$ reaches such a level at very early times, increasing with time by roughly two orders of magnitude and then slowly decreasing down to $W_{\mathcal{F}} \simeq 10^{-6}$. The energy radiated at ω_p is at all times significantly larger for the inhomogeneous plasma case, even if asymptotically $W_{\mathcal{F}h}$ and $W_{\mathcal{F}}$ reach the same amplitude. It is clear at this stage that processes specifically connected to the presence of density fluctuations strongly enhance fundamental emissions.

Figures 5(c) and (d) present the time variations of $W_{\mathcal{F}}$, $W_{\mathcal{F}h}$, $W_{\mathcal{M}}$, and $W_{\mathcal{M}h}$, as well as of the energies $W_{\mathcal{H}}$ and $W_{\mathcal{H}h}$ corresponding to the harmonic emissions at $2\omega_p$ (Krafft & Savoini 2021). For $\Delta N = 0.05$ (Figure 5(d)), fundamental emission dominates during the first stage of evolution ($\omega_p t \lesssim 2000$); then, for $\omega_p t \gtrsim 2000$, it is overcome by harmonic emission whose growth follows that of $W_{\mathcal{M}}$; asymptotically, $W_{\mathcal{H}}$ is one order of magnitude larger than $W_{\mathcal{F}}$. For $\Delta N = 0$ (Figure 5(c)), both $W_{\mathcal{F}h}$ and $W_{\mathcal{H}h}$ are continuously growing, with $W_{\mathcal{H}h}$ exceeding $W_{\mathcal{F}h}$ at any time. At $\omega_p t \simeq 3000$, i.e., much before the asymptotic time, $W_{\mathcal{H}h}$ has already reached about half of $W_{\mathcal{M}h}$. Note the significant contribution, at early times, of electromagnetic emissions radiated at frequencies different from ω_p and $2\omega_p$.

The time variations of the ratios $W_{\mathcal{F}}/W_{\mathcal{H}}$ and $W_{\mathcal{F}h}/W_{\mathcal{H}h}$ of the fundamental to the harmonic energies are shown in Figure 5(e). For the homogeneous plasma, $W_{\mathcal{F}h}/W_{\mathcal{H}h}$ varies around a quasiconstant value $\sim 10^{-2}$. When the plasma is inhomogeneous with $\Delta N = 0.05$, $W_{\mathcal{F}}/W_{\mathcal{H}}$ decreases over almost two orders of magnitude, reaching asymptotically 10^{-1}. In both cases, harmonic emission dominates at large times. Finally, Figure 5(f) presents the time variations of the ratios $W_{\mathcal{F}}/W_{\mathcal{L}}$ and $W_{\mathcal{F}h}/W_{\mathcal{L}h}$ of the fundamental electromagnetic to the total Langmuir energies. At any time, the fraction of Langmuir energy transformed into electromagnetic energy radiated at ω_p is larger when the plasma is

inhomogeneous. Indeed, $W_{\mathcal{F}}/W_{\mathcal{L}}$ mostly exceeds $W_{\mathcal{F}h}/W_{\mathcal{L}h}$ by more than two orders of magnitude; asymptotically, this difference is reduced, due mainly to the enhancement of harmonic emission when the plasma is homogeneous.

4. Conclusion

Two-dimensional PIC simulations are performed to study the generation of Langmuir wave turbulence by a weak electron beam in a randomly inhomogeneous plasma and its subsequent electromagnetic radiation, in conditions relevant to type III solar radio bursts. They use physical and numerical parameters that were not reached previously, providing spectral distributions of unprecedented accuracy and resolution, and evidencing electromagnetic waves with wave vectors down to $k\lambda_D \sim 0.001$.

This Letter shows for the first time the essential impact of random density fluctuations of average levels of a few percents of the background plasma on the characteristics of electromagnetic emission at the fundamental plasma frequency ω_p. It demonstrates that actually not only wave nonlinear interactions but also processes of Langmuir waves' transformations on the fluctuating inhomogeneities contribute to the generation of such emissions. The electromagnetic wave spectra at ω_p evidence a quasicircular shape that is significantly scattered and asymptotically isotropized by the density fluctuations whereas exhibiting a dipolar radiation pattern when the plasma is homogeneous.

In addition, this work shows the joint time evolution of electromagnetic waves radiated at fundamental ω_p and harmonic $2\omega_p$ frequencies, in a plasma with or without density fluctuations. In the homogeneous case, harmonic emission dominates over fundamental emission during all evolution whereas when the plasma contains density fluctuations, the latter is strongly dominant during several thousands of plasma periods before being overcome by the former when the total electromagnetic energy begins to saturate.

The impact of density fluctuations on the fundamental emission is already effective before the Langmuir wave energy has reached saturation. Indeed, at this stage and during beam relaxation, the amount of electromagnetic energy radiated at ω_p strongly exceeds that observed in the absence of density fluctuations. Nevertheless, asymptotically, the amplitudes of these emissions become roughly the same whether the plasma is homogeneous or not, due mainly to the dynamics of Langmuir wave turbulence during its saturation stage and of the beam.

Finally, the fraction of Langmuir wave energy involved in the generation of electromagnetic emissions at ω_p saturates around 10^{-4}, i.e., one order of magnitude above that reached when the plasma is homogeneous.

The role of the nonlinear wave-interaction mechanisms in the generation of electromagnetic emissions at ω_p will be discussed in more detail in a forthcoming paper. In particular, the impact of the density fluctuations on the dynamics and the intensity of the ion acoustic waves involved in these processes will be studied.

ORCID iDs

C. Krafft ⬚ https://orcid.org/0000-0002-8595-4772

References

Cairns, I. H., & Willes, A. J. 2005, PhPl, 12, 052315
Celnikier, L. M., Harvey, C. C., Jegou, R., Moricet, P., & Kemp, M. 1983, A&A, 126, 293
Derouillat, J., Beck, A., Perez, F., et al. 2018, CoPhC, 222, 351
Field, G. B. 1956, ApJ, 124, 555
Ginzburg, V., & Zheleznyakov, V. 1958, SvA, 2, 653
Kasaba, Y., Matsumoto, H., & Omura, Y. 2001, JGR, 106, 18693
Krafft, C., & Savoini, P. 2021, ApJL, 917, L23
Krafft, C., & Volokitin, A. S. 2020, PPCF, 62, 024007
Krafft, C., Volokitin, A. S., & Krasnoselskikh, V. V. 2013, ApJ, 778, 111
Krafft, C., Volokitin, A. S., & Krasnoselskikh, V. V. 2015, ApJ, 809, 176
Krupar, V., Maksimovic, M., Kontar, E. P., et al. 2018, ApJ, 857, 82
Lee, S.-Y., Ziebell, L. F., Yoon, P. H., et al. 2019, ApJ, 871, 74
Li, B., Willes, A. J., Robinson, P. A., & Cairns, I. H. 2005, PhPl, 12, 052324
Melrose, D. B. 1980, SoPh, 67, 357
Papadopoulos, K., Goldstein, N. L., & Smith, R. A. 1974, ApJ, 190, 175
Pritchett, P. L., & Dawson, J. M. 1983, PhFl, 26, 1114
Reid, H. A. S., & Ratcliffe, H. 2014, RAA, 14, 773
Rhee, T., Woo, M., & Ryu, C. M. 2009, JKPS, 54, 313
Thurgood, J. O., & Tsiklauri, D. 2015, A&A, 584, A83
Volokitin, A. S., & Krafft, C. 2018, ApJ, 868, 104
Volokitin, A. S., & Krafft, C. 2020, ApJL, 893, L47
Yin, L., Ashour-Abdalla, M., El-Alaoui, M., Bosqued, J. M., & Bougeret, J. L. 1998, GeoRL, 25, 2609
Yoon, P. H., Yi, S., & Ryu, C. M. 2005, PhP1, 12, 052305
Ziebell, L. F., Yoon, P. H., Petruzzellis, L. T., Gaelzer, R., & Pavan, J. 2015, ApJ, 806, 237